Systems analysis of the single photon response in invertebrate photoreceptors

Alain Pumir[†], Jennifer Graves[‡], Rama Ranganathan[‡], and Boris I. Shraiman[§¶]

[†]Laboratoire J. A. Dieudonne, Centre National de la Recherche Scientifique and Université de Nice, 06108 Nice, France; [‡]Green Center Division for Systems Biology and Department of Pharmacology, University of Texas Southwestern Medical Center, Dallas, TX 75390-9050; and [§]Kavli Institute for Theoretical Physics and Department of Physics, University of California, Santa Barbara, CA 93106

Edited by Charles F. Stevens, Salk Institute for Biological Studies, La Jolla, CA, and approved May 4, 2008 (received for review January 9, 2008)

Photoreceptors of *Drosophila* compound eye employ a G protein-mediated signaling pathway that transduces single photons into transient electrical responses called ''quantum bumps'' (QB). Although most of the molecular components of this pathway are already known, the system-level understanding of the mechanism of QB generation has remained elusive. Here, we present a quantitative model explaining how QBs emerge from stochastic nonlinear dynamics of the signaling cascade. The model shows that the cascade acts as an ''integrate and fire'' device and explains how photoreceptors achieve reliable responses to light although keeping low background in the dark. The model predicts the nontrivial behavior of mutants that enhance or suppress signaling and explains the dependence on external calcium, which controls feedback regulation. The results provide insight into physiological questions such as single-photon response efficiency and the adaptation of response to high incident-light level. The system-level analysis enabled by modeling phototransduction provides a foundation for understanding G protein signaling pathways less amenable to quantitative approaches.

G protein-coupled receptor pathway | phototransduction | quantitative modeling

Signal transduction is one of the fundamental functions of the cell. It invariably involves a protein receptor specialized for a certain stimulus and a cascade of molecular transformations typically leading to a macroscopic change in the state of the cell. Understanding signal transduction requires more than knowing the molecular components of the pathway. One also needs to understand sensitivity, noise, spatial localization, dynamic range and adaptation—a plethora of quantitative features—that characterize the system-level function of the signaling pathway. *Drosophila* phototransduction is a signaling system of unmatched experimental tractability. It offers a readily controllable stimulus (light) and a readily accessible output (electric depolarization that can be accurately measured for single cells) as well as access to numerous mutants with interesting phenotypes and a possibility to perturb the system by manipulating the ionic composition of the buffer solution. This makes possible a quantitative experimental characterization and provides a unique opportunity to develop and test quantitative modeling approaches. Below, after describing *Drosophila* phototransduction, we present, analyze, and discuss a quantitative model of this pathway and its dynamic behavior.

The single-photon response of a *Drosophila* photoreceptor cell involves coordinated opening of 15–20 ion channels (1), which corresponds to ≈15 pA inward current for 20 ms (Fig. 1*a*). Individual quantum bumps (QBs) under physiological conditions have a largely stereotypic shape (1), but they occur with a variable delay (or ''latency'') after light stimulus (Fig. 1*a*), suggesting that phototransduction cascade transforms single-photon absorption into a regenerative, nonlinear depolarization event.

The major biochemical steps of the signaling cascade underlying invertebrate phototransduction (2–7) are shown in Fig. 1*b*. Absorption of a photon by rhodopsin (R) leads to formation of the active state (metarhodopsin, M*) that catalyzes nucleotide exchange on the α-subunit of a heterotrimeric G_q protein. $G_{q\alpha}$-GTP then activates a PLCβ molecule that catalyses hydrolysis of PIP_2 and releases diacylglycerol, DAG (6). DAG causes coordinated opening of TRP and TRP-like (TRPL) channels (4, 7–9); which results in an influx of Na^+ and Ca^{2+} ions and the transient depolarization of the cell membrane called the QB. Shutoff of the activated intermediates consists of several reactions: (*i*) M* deactivation by binding of arrestin—the inhibitory protein (10, 11); (*ii*) deactivation of PLCβ after GTP hydrolysis in the active $G_{q\alpha}$-GTP-PLCβ complex; and (*iii*) degradation of DAG initiated by DAG kinase (4).

Ca^{2+} plays a key role in photoreceptor function. Ca^{2+} influx during a QB causes a 1,000-fold transient increase of internal concentration $[Ca^{2+}]_{in}$ (12, 13) [in a tiny microvillus where signaling takes place (2)] that drives a sequential positive and negative feedback determining the shape and size of the QB (1). The threshold for positive feedback is lower than that for negative feedback, so that initial elevation of $[Ca^{2+}]_{in}$ facilitates opening of more TRP channels and increases the rate of Ca^{2+} influx. At higher $[Ca^{2+}]_{in}$, negative feedback drives rapid closing of TRP channels and shut-off of the PLCβ activity, thereby terminating the response (2). The molecular details of the positive feedback are still unknown. The negative feedback is mediated by several Ca^{2+}-dependent processes, including phosphorylation of several proteins by Ca^{2+}–calmodulin-dependent protein kinase (CamK) (2, 14, 15) and by eye-specific protein kinase C (ePKC) (16, 17).

Results

Model Formulation. To understand quantitatively how a QB is generated, we formulated a theoretical model that describes the key processes of phototransduction. It is most easily rendered in terms of kinetic equations (see *Methods*). However, because many of the participating molecules occur in small numbers, stochastic fluctuation in numbers of activated molecules cannot be neglected. Thus, we reinterpreted the system of kinetic equations as a master equation (18) describing the probability of finding a given number of molecules of a certain type [see supporting information (SI) *Text*]. The stochastic model is then studied by using numerical simulations based on the Gillespie algorithm (19). The model parameters were obtained by fitting to three features of the WT QB: the average waveform, the mean latency, and the coefficient of variation of the QB amplitude (Fig. 1*b* and *SI Text*) and by imposing two additional constraints requiring that the average number of PLC* molecules involved in generating a WT QB is close to five (3) and that response at $[Ca^{2+}]_{ex} = 0$ is weak compared with a normal QB. The choice of parameters, their role in controlling particular features of the response, and the sensitivity analysis for the fit are

Author contributions: A.P., R.R., and B.I.S. designed research; A.P., J.G., R.R., and B.I.S. performed research; and A.P., R.R., and B.I.S. wrote the paper.

The authors declare no conflict of interest.

This article is a PNAS Direct Submission.

¶To whom correspondence should be addressed. E-mail: shraiman@kitp.ucsb.edu.

This article contains supporting information online at www.pnas.org/cgi/content/full/0711884105/DCSupplemental.

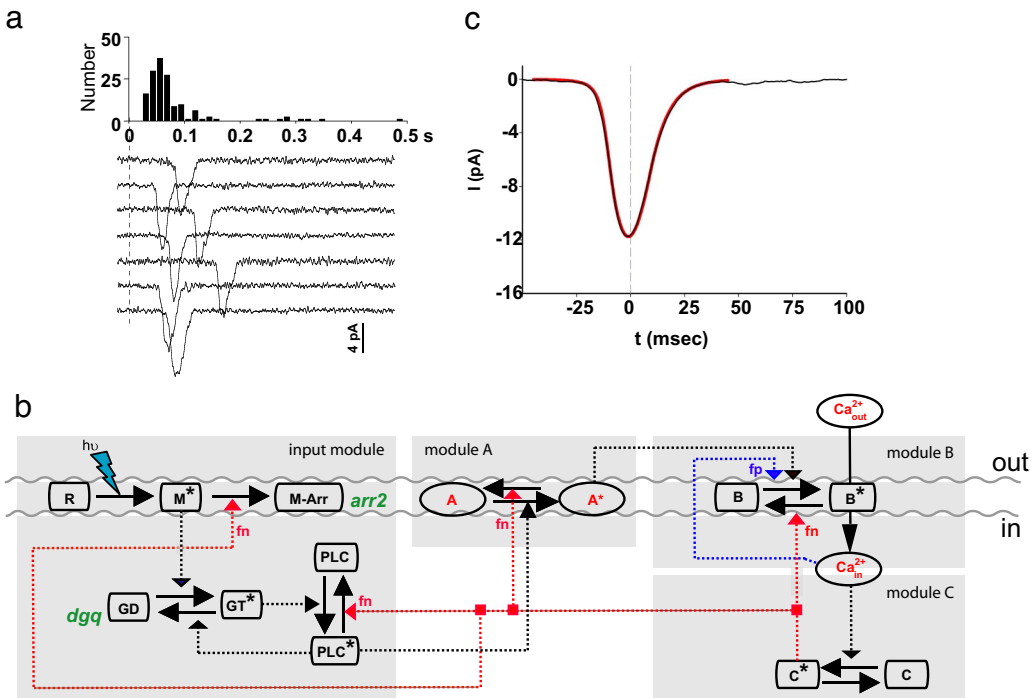

Fig. 1. QBs and the phototransduction cascade. (*a*) QBs, generated by a brief flash of dim light and recorded by using whole-cell voltage clamp from isolated WT photoreceptor cells. The traces show a brief (≈20 ms) and intense (≈20 pA) inward current. Significant variability is observed, in particular in latency, the histogram of which is shown at the top. (*b*) Simplified view of the molecular mechanism of invertebrate phototransduction. Absorption of a photon by rhodopsin, via G proteins, activates PLCβ (input module), which generates DAG, which directly or indirectly acts as the activator A* (module A) leading to the opening of TRP channels (B*). The opening of channels is facilitated by the rapid influx of Ca^{2+} that acts as a positive feedback (fp) comprising module B. At higher concentration, Ca^{2+} acts via a Ca-binding intermediary (C*) providing the negative feedback (fn) in module C, which terminates the QB. (*c*) The average profile of aligned QBs. The black curve shows the average of 83 measured QBs, the red one is the model fit.

discussed at length in *SI Text*; see also Fig. S3. However, the results presented here regarding the mechanism of QB generation are not limited to any particular choice of parameters. Instead, our analysis identifies the conditions necessary for QB generation which, provided certain essential features of the cascade (such as a rapid positive feedback), are satisfied in a wide region of parameter space.

An important issue in developing the model is to properly represent the still incomplete knowledge of certain molecular details in fly phototransduction. First, although PLCβ activity and DAG is clearly required, the exact molecular mechanism of TRP channel activation is still uncertain (8). Thus, in the model, we simply refer to the activator of channels by a variable A*, which is produced upon PLCβ activation and degraded by the Ca^{2+}-dependent inhibitory processes. Second, two kinds of TRP channels operate in *Drosophila* photoreceptors but for simplicity, we lump these together in the variable B. Following the convention that starred species are the activated states, open channels are referred to as B^*. Finally, several Ca^{2+}-dependent inhibitory mechanisms likely operate in the photoreceptor cell. In the absence of more detailed information, here, we combine these processes together in a single dynamical variable, C^*. These choices obviously ignore some of the system complexity, but they provide a practical approximation for assessing the experimental consistency of the model. We can think of A^*, B^* and C^* variables as phenomenological outputs of three essential "modules" comprising the cascade: (*i*) an "activation module" downstream of PLCβ but upstream of the channels, (*ii*) a "bump-generation module" including channels and the Ca-mediated positive feedback and (*iii*) the Ca^{2+}-dependent "negative-feedback module" (Fig. 1*b*).

Fig. 2*a* shows that QB generation in the model is a dynamic "integrate-and-fire" process. In the initial period after M* activation and before channels have opened, Ca^{2+}-dependent inhibition is absent and A^* is relatively stable. Therefore, PLCβ activity (PLC^*) makes A^* rise steadily until the channels open. What happens next depends on the level of A* at the moment when the first channel opens. If A* at that point exceeds a certain threshold level (A_{QB}, defined below), opening of a single channel is likely to trigger a regenerative burst of channel opening, a process that is facilitated by the positive feedback, see Eq. **6** in *Methods*. On the other hand, if A* stays below the threshold when the first channel opens, this burst is unlikely to ignite. This condition for reliable QB generation is found to be satisfied in a specific region of the PLC^*–$[Ca^{2+}]_{ex}$ variable plane, shown in Fig. 2*c* (see *SI Text* and Fig. S1 for details). The region is delineated on one side (the blue line in Fig. 2*c*) by the requirement that $[Ca^{2+}]_{ex}$ is sufficiently high for the Ca^{2+} influx through a single open channel to enable positive feedback and on the other side (the red line) by the threshold condition $A_T > A_{QB}$. A_T is the typical level of A^* at the moment of the first channel opening, and A_{QB} is defined as the level of A^* at which the probability of opening the second channel equals the probability of closing the first. A_{QB} depends on the strength of positive feedback and increases with decreasing $[Ca^{2+}]_{ex}$ because lower $[Ca^{2+}]_{ex}$ weakens positive feedback. A_T, on the other hand, is determined by the PLC^*-dependent rate of A^* production: The faster A^* is produced, the higher it is when the first channel opens. The $A_T = A_{QB}$ line (red in Fig. 2*c*) corresponds to a cross-over between a regime where most channel-opening events fail to ignite a high-amplitude response to the regime where such failures are rare, and QBs are reliably generated.

In the model, the WT single-photon event typically generates $PLC^* \approx 5$ yielding QBs with a probability of ≈0.8. On the other hand we note that $PLC^* = 1$ even at physiological Ca^{2+} level is not sufficient for reliable QBs generation—a fact to which we shall return in discussing mutant phenotypes (Fig. 2*c*). For $[Ca^{2+}]_{ex}$ below the blue line in Fig. 2*c*, the positive feedback is too weak to trigger a QB and B^* follows A^* adiabatically resulting in a response with ≈3-fold lower peak amplitude and 5-fold slower time course. The cross-over region itself is more complex because it corresponds to the "excitable system" (20) behavior (described in *SI Text* and Figs. S1 and S2), where QB generation depends strongly on fluctuations in channel opening. As a result, the model predicts enhanced variability in the amplitude of the response at the edge of the QB domain. The cross-over behavior can be observed experimentally by systematically reducing Ca^{2+} concentration in the bath solution (1).

What determines QB shape and the variability in latency after

BIOPHYSICS

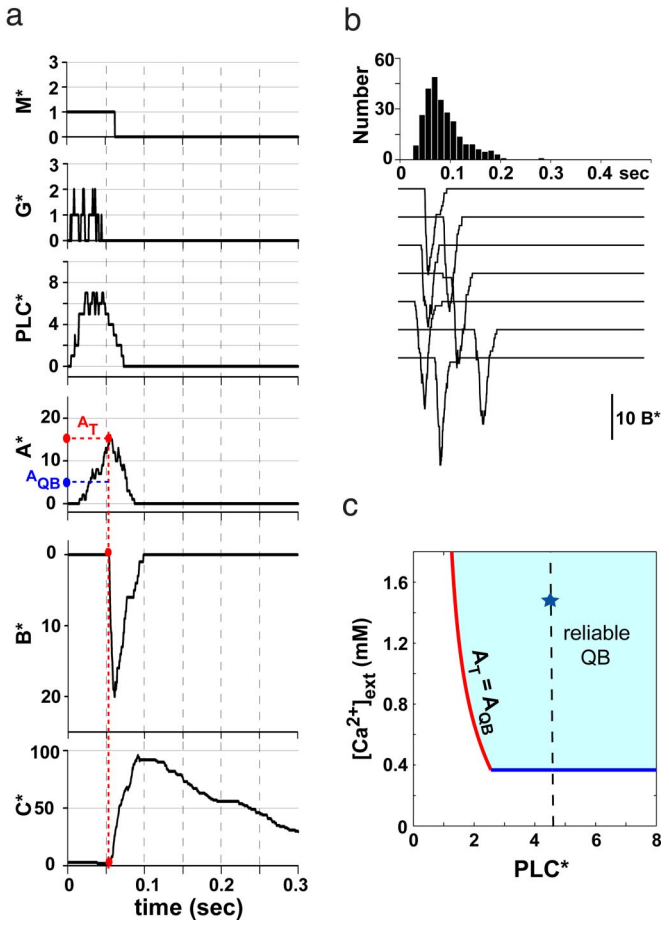

Fig. 2. Model of QB generation. (*a*) An example of temporal evolution of the key dynamical variables during a QB. The input module produces ≈5 PLC*, with significant fluctuations. The number of A* molecules rises slowly until it reaches the level A_T, when channels start opening rapidly (sharp increase of B*). The value of A_T is larger than A_{QB}, the threshold for generating reliable QB. The observed variability in latency, see *b*, is largely attributable to the fluctuations of the levels A_T at which the QB starts. Ultimately, the Ca-dependent inhibitor C* gets produced and terminates the QB. (*b*) Simulated QBs elicited by activation of a single M* at $t = 0$. A brief (≈20 ms) opening of ≈20 channels occurs after a latency of ≈80 ms. A significant variability can be seen from the traces, in particular in the latency time, whose distribution is shown at the top. (*c*) The domain of QB generation in the PLC*–$[Ca^{2+}]_{ex}$ plane defined by the condition that opening of a single channel will, with high probability, generate the opening of many more channels. The star denotes the operating point corresponding to the WT.

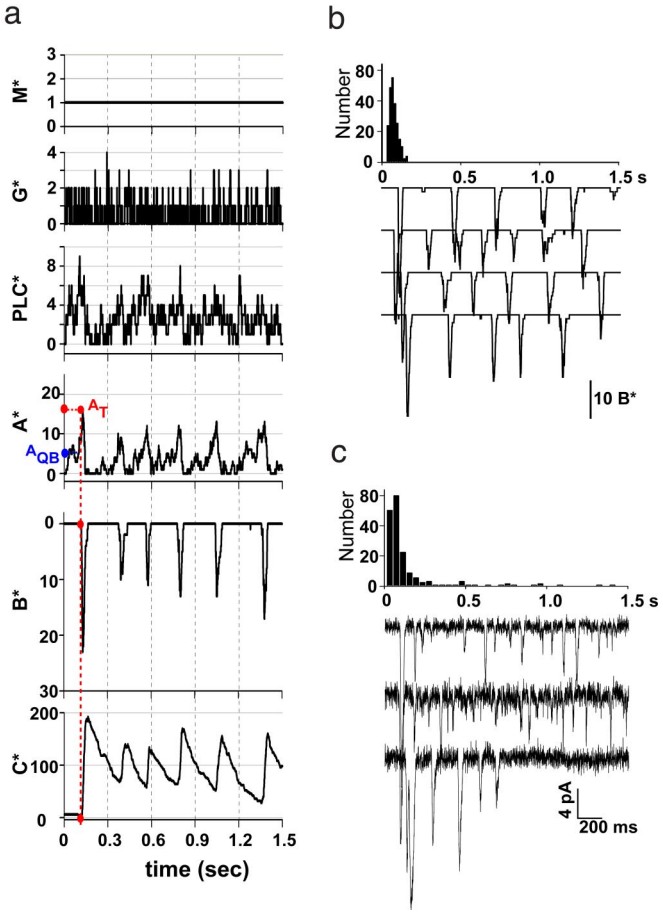

Fig. 3. Single photon response in the absence of metarhodopsin deactivation. (*a*) Simulated dynamics of key variables. M* stays on for the entire period shown. Generation of the first QB is similar to the WT case shown in Fig. 2*a*; however, as soon as C* goes down, PLC* and A* accumulate again, generating new QBs of smaller amplitude. The amplitudes and time delays between consecutive QBs fluctuate because of the stochastic nature of A* production, which triggers the next QB. (*b*) Simulated response to the persistent activity of a single M*. Latency distribution for the first QB, shown at the top, is similar to WT (compare with Fig. 2*b*). A significant variability is seen in the amplitude and in the time delay between consecutive QBs. (*c*) QB generated by a brief flash of dim light and recorded by using whole-cell voltage clamp from isolated *arr2*^{3} mutant photoreceptors. The observed response is in qualitative agreement with model predictions.

photon absorption? In the model, the stochastically varying delay in the appearance of the QBs (Fig. 2*b*) is mostly due to the trial-to-trial variability in the time it takes for A* to build-up to $A_T > A_{QB}$ after photon absorption. Variability in latency is significant because of the small number of activated *PLC**s but also because of the variation in the actual time when first channel opens. As to QB amplitude and duration, these parameters are determined by the rise of the inhibitor *C** upon channel opening, which provides the feedback signal to deactivate both *A**, *B**, and *M**, terminating the bump. A calculation of QB amplitude as a function of *PLC** and $[Ca^{2+}]_{ex}$ is given in the *SI Text*. Interestingly, *C** decays slowly after the QB occurs, predicting a period after a QB during which further signaling responses are suppressed. Such a "refractory period" has been proposed to play a critical role in allowing time for activated upstream intermediates such as metarhodopsin to shut off before the system returns to the resting dark state (2), a process that extends the dynamic range of vision.

Mutant Behaviors. A valuable test of the QB model is its ability to predict mutant phenotypes that nontrivially alter system behavior. For example, what happens if metarhodopsin fails to deactivate, and the system stays above threshold for quantum bump generation as *C** falls? Under conditions of persistent *M** and, therefore, *PLC** activation, the integrate-and-fire behavior in our model leads to a "relaxation oscillation," where ramps of *A** accumulation leading to QBs are followed by refractory periods during which inhibition, *C**, is gradually relaxed (see Fig. 3*a*). Because of the stochastic nature of the QB production, the QB "train" generated by this relaxation oscillator is far from periodic: The latency and the amplitude of secondary QBs depends on the exact *C** level left behind by the preceding QB. Thus, in the absence of *M** deactivation, the model predicts a train of irregularly spaced and sized QBs in response to a single photon (Fig. 3*b*). However, consistent with the fact that the initial activation event is normal, the model predicts that the distribution of response latencies should remain similar to that of the WT model.

The *arr2*^{3} mutation (10, 21) provides an opportunity to compare

predictions with experiment. These cells are hypomorphic for the major arrestin responsible for metarhodopsin shutoff and are known to display slowly inactivating light responses that are rate-limited by the inactivation of metarhodopsin. As predicted by the model, the slow shutoff of the light response in $arr2^3$ mutants comes, not from changes in QB shape, but in repeated, stochastic firings of small bumps after a normal-sized initial bump (14, 22) (Fig. 3*c*). The probability distribution of wait times for the first bump is, as predicted, the same as that for WT photoreceptor cells (compare Figs. 1*a* and 3*c*). The frequency of bump repetitions is clearly slower in the model in comparison with the data, suggesting further refinements of the model to accurately represent the rate of C^* deactivation (which controls the refractory period between bump generation events). Nevertheless, the basic consistency of experiment and prediction provides strong validation for the quantitative model for QB generation in fly photoreceptors.

To further test the predictive power of the model, we examined another mutant with well characterized QB defects. The mutant, dgq^1, is a hypomorphic allele displaying a ≈100-fold reduction in the $G_{q\alpha}$ subunit that couples metarhodopsin to PLCβ activation and therefore shows a dramatic reduction in the efficiency of signal activation (3). Indeed, dgq^1 mutants show reduced bump size, a severely broadened latency distribution (see Fig. 4*a*) and a nearly 3 log-order reduction in light sensitivity, factors that render these mutants nearly blind. Fig. 4 *a* and *b* shows simulations in which we reduced the total number of G proteins per microvillus to one (see Table S1 for the list of model parameters). Consistent with the experimental measurements, reducing G leads to a much prolonged latency of QB activation and a reduced QB amplitude. In addition, this single perturbation of the model also captures the poor efficiency of signaling; less than one in 200 simulated rhodopsin activations now produces a successful QB. This high failure rate of signaling is primarily explained in the model by the fact that activation in dgq^1 mutants amounts to production of a single PLC^* (Fig. 4*a*) that is unlikely to generate $A_T > A_{QB}$ before it itself deactivates. Thus, the long latency for the rare successful QBs reflects the long time it takes for a single PLC^* to build up sufficient A^*, and the low efficiency reflects the low probability for the activity of a single PLC^* to last that long.

Dependence on External Ca^{2+} Concentration. The external Ca^{2+} concentration can be readily varied in an experiment, as was done by Henderson *et al.* (1), who measured the mean QB amplitude and the corresponding coefficient of variation (i.e., the ratio between the root mean square variation and the mean) as well as the mean latency time for different $[Ca^{2+}]_{ex}$. As shown in Fig. 5, the model predicts that at low Ca^{2+} response amplitude remains essentially constant and small, but as the $[Ca^{2+}]_{ex}$ increases above a certain threshold, the average response amplitude goes up. This threshold corresponds to the Ca^{2+} level where positive feedback becomes important, and the system crosses over from passive to regenerative response—the basic systems-level property that defines the QB. The coefficient of variation peaks as this cross-over occurs, because in the cross-over regime, the response is bimodal; a photon either triggers the passive event, causing a slow, small response or a regenerative event, causing a fast, large response (see *SI Text* and Fig. S2). At $[Ca^{2+}]_{ex}$ >0.5 mM, the negative feedback becomes important, reducing the peak number of open channels. The trends shown in Fig. 5 are generally consistent with the results of Henderson *et al.* (1), including, in particular, the peak in the coefficient of variation. On the other hand, the dependence of the latency time on $[Ca^{2+}]_{ex}$ predicted by the model appears to be too weak, suggesting that the present model with its emphasis on simplification incompletely represents the Ca^{2+} dependence for some of the processes involved in module *A*.

Light Adaptation. The mathematical model can be used to provide insight into interesting physiological processes such as adaptation of

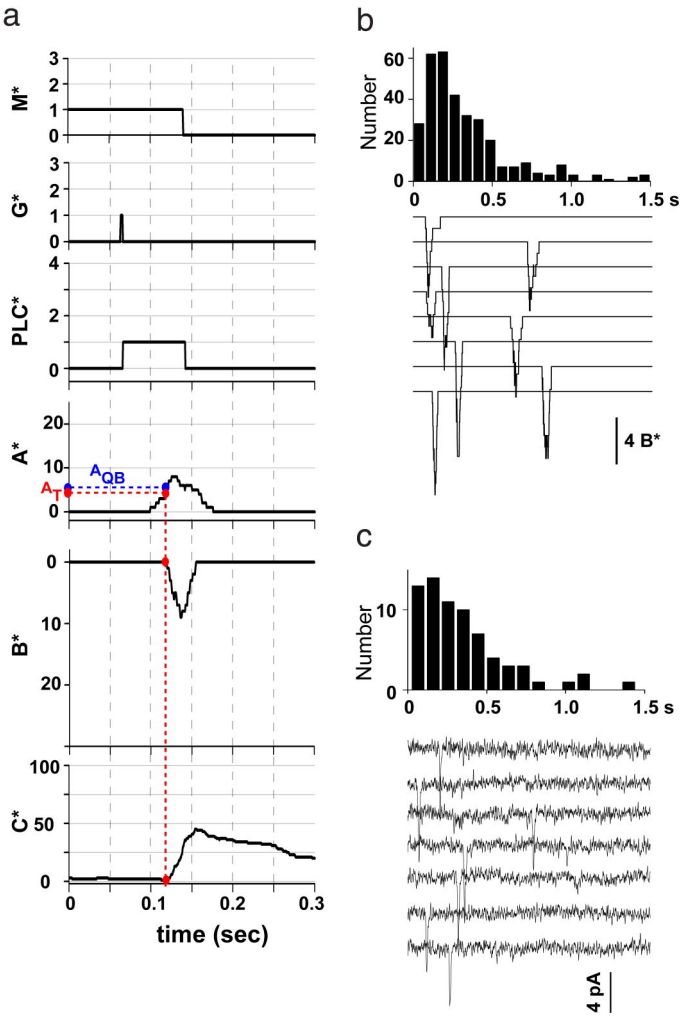

Fig. 4. Single-photon response of $G_{q\alpha}$-protein hypomorphic receptors. (*a*) An example of temporal evolution of the dynamical variable during the successful generation of a QB. The excitation of a single G protein leads to the activation of a single PLC*, which leads to QB activation only in rare instances when PLC* does not spontaneously deactivate before generating enough A* to ignite a QB. (*b*) Simulation of the model with a single G protein per microvillus. QBs shown occur once in ≈200 trials. The amplitude of the QB is reduced and the latency increased compared with WT. (*c*) Measured response of dgq^1 mutant cells to dim light. QB have a reduced amplitude (≈5 pA), ≈5-fold longer latency and occur with ≈1,000-fold lower probability compared with the WT.

the response at higher light levels. To extend the analysis from single photons to macroscopic light flashes we shall assume that photon absorption events are randomly distributed among the ≈30,000 microvilli, and the resulting QB currents are linearly summed in the photoreceptor cell soma. The shape of the macroscopic response is then determined by the convolution of the average QB shape with the latency distribution (1) (see Fig. 6). Response is expected to deviate from linearity once the number of absorbed photons per flash becomes comparable with the number of microvilli so that a significant fraction of microvilli are activated by more than one photon. Absorption of multiple photons by a single microvillus is described by the Poisson distribution and leads to sublinearity of response at high flash intensity (Fig. 6 *Inset*). The extent of sublinearity and saturation depends on the (average) fraction of the total number of TRP channels open during the QB relative to the total number of channels in the microvillus—one of the parameters of the model. Interestingly, as shown in Fig. 6*b*, the model predicts that the onset of sublinearity in the response should be accompa-

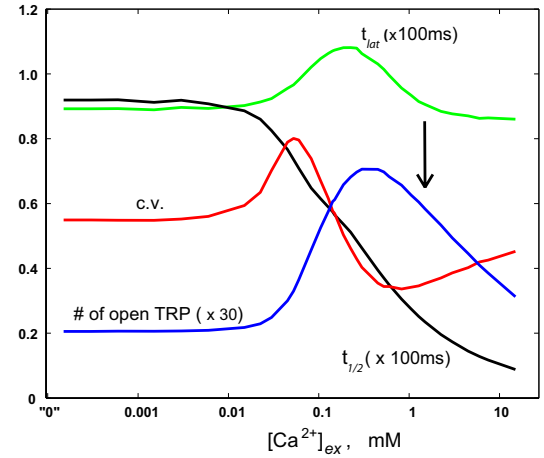

Fig. 5. Predicted dependence of single-photon response on $[Ca^{2+}]_{ex}$. Blue line, the mean amplitude of simulated single photon response; red line, the coefficient of variation (i.e., ratio of the root mean square variation to the mean amplitude). Note the peak in the coefficient of variation marking the cross-over to the QB regime. Black line, average response half-width; green line, average response latency. Physiological $[Ca^{2+}]_{ex}$ = 1.5 mM is shown by the vertical arrow.

nied by a reduction in latency. This reduction of latency is due to the accelerated rise of A^* caused by the multiple activation in the input module.

Discussion

The mathematical model developed above is not intended to represent every biochemical detail of the phototransduction cascade; such a model would require many more kinetic parameters than can be justified by our current knowledge of this system. Instead, by resorting to simple and generic parameterizations, the model bridges the most essential gap in our understanding of this system at the current time—the origin of the elementary visual response in the global dynamics of the signaling process. These simplifications enhance our ability to productively iterate between experiment and theory and suggest a paradigm for analysis of this G protein signaling system. For example, in lieu of detailed knowledge about the molecular details of TRP channel activation and positive feedback, we introduced a cooperatively acting and Ca^{2+}-dependent activator A^*. In a detail-independent way, this approach provides extensive quantitative insight into nonintuitive properties of the signaling dynamics relating for example the QB yield—the probability of generating a QB in response to activation of a single rhodopsin—to specific aspects of G protein and PLCβ activation, DAG production and Ca^{2+}-dependent TRP channel opening. Virtual mutagenesis studies can now provide predictions about how modulation of any of these steps influence QB yield and will help to optimize the design of experiments that can test these predictions. In this regard, it is reassuring that the parameter set determined in this work results in a QB yield of $\approx$0.8, consistent with the $>$0.5 yield that is expected on the basis of the experimental data for *Musca* photoreceptor cells (23).

The model-based analysis of the dgq^1 mutant behavior provides insight into how *Drosophila* photoreceptor cells suppress spurious signaling in the dark. It has been noted that small QB-like events can occur spontaneously in the dark and have been interpreted as thermal activation of single G proteins (3). The discussion above suggests that only a small fraction of events where a G protein or a PLCβ is spontaneously activated result in a QB. Spontaneous opening of TRP channels should also contribute to "dark noise," but most of these would be limited to single channel events; the probability of a QB generation upon opening a single channel is reduced by a factor $(A_{\mathrm{Dark}}/A_{QB})^m$, where A_{Dark} is the level of

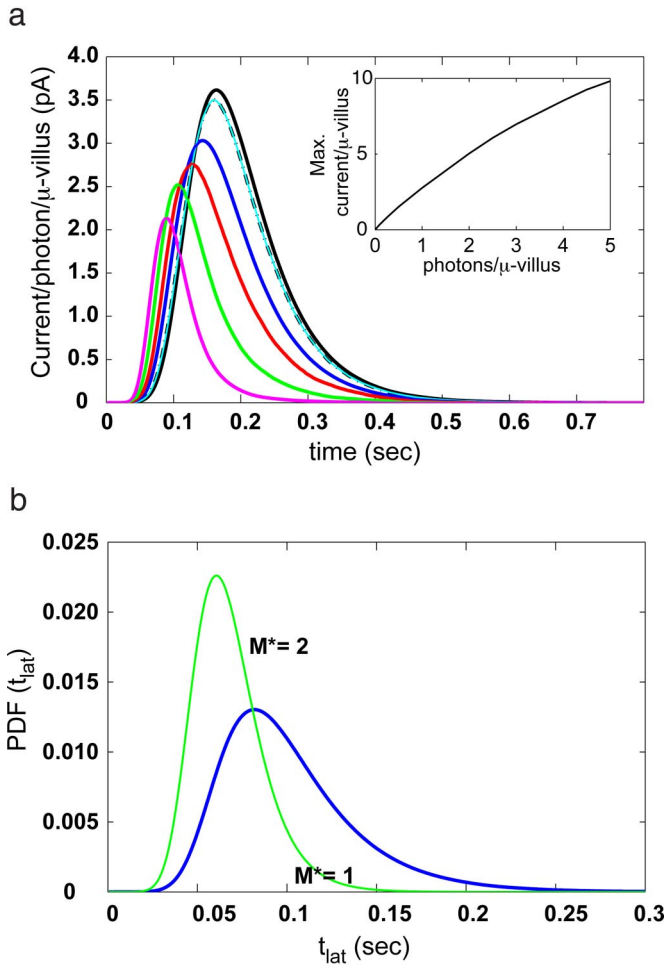

Fig. 6. Predicted macroscopic response as a function of light flash intensity. (*a*) Model predictions for the average current response per absorbed photon for flashes of different intensity. Light flashes are assumed to result in a Poisson-distributed number of absorbed photons. Color denotes the mean number of absorbed photons photon per microvillus: 0.1 (cyan), 0.5 (blue), 1 (red), 2 (green), and 4 (magenta). The black curve shows the averaged response to a single absorbed photon. (*Inset*) Peak amplitude of the macroscopic response as a function of flash intensity. (*b*) Latency distribution for a QB induced by single (blue) and double (green) metarhodopsin activation event. Simultaneous activation of multiple metarhodopsin molecules reduces the latency of QB generation.

activator in the dark. Thus, the nonlinearity of the QB generation process suppresses the effect of the inevitable spontaneous activation of signaling intermediates. Such a process should contribute to optimizing the signal-to-noise ratio of photoreceptor cells operating under low-light conditions.

It is interesting to compare *Drosophila* and, more generally, invertebrate phototransduction with the vertebrate system. The two systems part their ways just beyond the input stage, which in both cases employs rhodopsin and G proteins. In contrast to *Drosophila*, vertebrate phototransduciton involves a phosphodiesterase and a cGMP-gated channel (24–26). Although Ca^{2+} plays a role in negative feedback and light adaptation, single-photon response does not have the regenerative nature of a QB, so that at low light, vertebrate phototransduction seems to be "engineered" as an analog amplifier (27). It would be interesting to understand evolutionary pressures and constraints that explain the striking difference in the way vertebrates and invertebrates deal with light. For now, this remains an open question.

Going beyond the light response, *Drosophila* phototransduction has served as a general model system for phosphoinositide signaling. There are close functional analogies at the systems level for many of the underlying processes (G protein-coupled receptor desensitization, arrestin function in the inactivation of the receptor, and an adapter molecule for endocytosis, scaffolding, PLC-β feedback onto Gq, and regulation of apoptosis), and there are obvious molecular homologies in that none of the molecules involved are unique to fly vision (28). An example of a closely homologous system is provided by the mammalian taste (sweet, bitter, and umami) receptor cells (29). Yet presently, we know too little about the elemental physiological response in these systems to say whether they function in the regime similar to or very different from invertebrate phototransduction.

In summary, the theoretical and experimental studies described above provide a quantitative model for the basic unit of phototransduction response, the QB. The availability of such a model for an experimentally powerful system such as *Drosophila* photoreceptor cell provides a framework for a systems-level analysis of a prototypical G protein-mediated signaling network.

Methods

Modeling. The mathematical model was based on the following chemical kinetics equations:

$$\frac{dM^*}{dt} = -\gamma_{Rh^*}(1 + g_{Rh^*}f_n)M^* \quad [1]$$

governs deactivation of metarhodopsin (M*).

$$\frac{dG}{dt} = -\kappa_{G^*}G \times M^* + \gamma_{Gi}(G_T - G - G^*) \quad [2]$$

$$\frac{dG^*}{dt} = \kappa_{G^*}G \times M^* - \kappa_{PLC^*}PLC_T \times G^* \quad [3]$$

describe activation and inactivation of G protein—*G** and *G* being, respectively, its active and resting forms. G_T is the total number of G proteins in the microvilli.

$$\frac{dPLC^*}{dt} = \kappa_{PLC^*}PLC_T \times G^* - \gamma_{PLC^*}(1 + g_{PLC^*}f_n)PLC^* \quad [4]$$

$$\frac{dA^*}{dt} = \kappa_{A^*}PLC^* - \gamma_{A^*}(1 + g_{A^*}f_n)A^* \quad [5]$$

describe activation and inactivation of *PLC*β and production and degradation of the activator molecule *A**. *PLC** is the number of active molecules, whereas PLC_T is the total number.

$$\frac{dB^*}{dt} = \kappa_{B^*}(1 + g_{B^*,p}f_p) \times (A^*/K_{A^*})^m(B_T - B^*) - \gamma_{B^*}(1 + g_{B^*,n}f_n)B^* \quad [6]$$

describes opening and closure of TRP channels denoted (in the open form) by B*; B_T is the total number of channels. Opening and closure of channels are facilitated, respectively, by the positive, f_p, and negative, f_n, feedback defined below.

$$\frac{d[\mathrm{Ca}]}{dt} = \sigma B^*([\mathrm{Ca}]_{\mathrm{ext}} - [\mathrm{Ca}]) - \gamma_{\mathrm{Ca}}([\mathrm{Ca}] - [\mathrm{Ca}]_0) - (\kappa_{C^*}[\mathrm{Ca}] - \gamma_{C^*}[C^*]) \quad [7]$$

$$\frac{dC^*}{dt} = \kappa_{C^*}Ca - \gamma_{C^*}C^* \quad [8]$$

describe Ca^{2+} balance and the dynamics of the Ca-dependent mediator of negative feedback (C*). Positive and negative Ca-dependent feedbacks were parameterized by Hill functions f_p(Ca), and f_n(*C**) are defined by

$$f_p(\mathrm{Ca}) = \frac{([\mathrm{Ca}]/K_p)^{m_p}}{1 + ([\mathrm{Ca}]/K_p)^{m_p}} \quad [9]$$

$$f_n(C^*) = \frac{([C^*]/K_n)^{m_n}}{1 + ([C^*]/K_n)^{m_n}}. \quad [10]$$

The numerical values of all of the parameters in Eqs. (**1**-**10**) are given in Table S1. Simulation was based on a Gillespie algorithm and was carried out on a PC using custom Matlab and Fortran programs, available upon request.

Experiment. Fly stocks used in this work were *Canton S* (*CS*), *cn dgq*[1], and *w;;arr2*[3]. Whole-cell recordings used retinas from newly eclosed flies that were prepared as described (11, 16). For more information, see *SI Text*.

ACKNOWLEDGMENTS. This work was supported by National institutes of Health (NIH) Grant R01-GM65396 (to B.I.S.), the Robert A. Welch Foundation (to R.R.), and the Mallinckrodt Foundation Scholar Award (to R.R.). J.G. was supported in part by NIH Grant T32-GM008014 to the University of Texas Southwestern Medical Scientist Training Program.

1. Henderson SR, Reuss H, Hardie RC (2000) Single photon responses in *Drosophila* photoreceptors and their regulation by Ca^{2+}. *J Physiol* 524 Pt 1:179–194.
2. Hardie RC, Raghu P (2001) Visual transduction in *Drosophila*. *Nature* 413:186–193.
3. Hardie RC, *et al.* (2002) Molecular basis of amplification in *Drosophila* phototransduction: Roles for G protein, phospholipase C, and diacylglycerol kinase. *Neuron* 36:689–701.
4. Hardie RC (2003) TRP channels in *Drosophila* photoreceptors: the lipid connection. *Cell Calcium* 33:385–393.
5. Ranganathan R, Malicki DM, Zuker CS (1995) Signal transduction in *Drosophila* photoreceptors. *Annu Rev Neurosci* 18:283–317.
6. Scott K, Becker A, Sun Y, Hardy R, Zuker C (1995) Gq alpha protein function *in vivo*: Genetic dissection of its role in photoreceptor cell physiology. *Neuron* 15:919–927.
7. Scott K, Zuker C (1998) TRP, TRPL and trouble in photoreceptor cells. *Curr Opin Neurobiol* 8:383–388.
8. Chyb S, Raghu P, Hardie RC (1999) Polyunsaturated fatty acids activate the *Drosophila* light-sensitive channels TRP and TRPL. *Nature* 397:255–259.
9. Raghu P, *et al.* (2000) Constitutive activity of the light-sensitive channels TRP and TRPL in the *Drosophila* diacylglycerol kinase mutant, rdgA. *Neuron* 26:169–179.
10. Dolph PJ, *et al.* (1993) Arrestin function in inactivation of G protein-coupled receptor rhodopsin *in vivo*. *Science* 260:1910–1916.
11. Ranganathan R, Stevens CF (1995) Arrestin binding determines the rate of inactivation of the G protein-coupled receptor rhodopsin *in vivo*. *Cell* 81:841–848.
12. Oberwinkler J, Stavenga DG (2000) Calcium transients in the rhabdomeres of dark- and light-adapted fly photoreceptor cells. *J Neurosci* 20:1701–1709.
13. Oberwinkler J (2002) Calcium homeostasis in fly photoreceptor cells. *Adv Exp Med Biol* 514:539–583.
14. Scott K, Zuker C (1997) Lights out: Deactivation of the phototransduction cascade. *Trends Biochem Sci* 22:350–354.
15. Arnon A, Cook B, Montell C, Selinger Z, Minke B (1997) Calmodulin regulation of calcium stores in phototransduction of *Drosophila*. *Science* 275:1119–1121.
16. Ranganathan R, Harris GL, Stevens CF, Zuker CS (1991) A *Drosophila* mutant defective in extracellular calcium-dependent photoreceptor deactivation and rapid desensitization. *Nature* 354:230–232.
17. Hardie RC, *et al.* (1993) Protein kinase C is required for light adaptation in *Drosophila* photoreceptors. *Nature* 363:634–637.
18. van Kampen NG (1981). *Stochastic Processes in Physics and Chemistry* (North–Holland, Amsterdam).
19. Gillespie DT (1976) General method for numerically simulating stochastic time evolution of coupled chemical reactions. *J Comp Phys* 22:403–434.
20. Murray J (2002) *Mathematical Biology* (Springer, Berlin).
21. LeVine H, III, *et al.* (1990) Isolation of a novel visual-system-specific arrestin: an *in vivo* substrate for light-dependent phosphorylation. *Mech Dev* 33:19–25.
22. Scott K, Sun Y, Beckingham K, Zuker CS (1997) Calmodulin regulation of *Drosophila* light-activated channels and receptor function mediates termination of the light response *in vivo*. *Cell* 91:375–383.
23. Dubs A, Laughlin SB, Srinivasan MV (1981) Single photon signals in fly photoreceptors and first order interneurones at behavioral threshold. *J Physiol* 317:317–334.
24. Stryer L (1986) Cyclic GMP cascade of vision. *Annu Rev Neurosci* 9:87–119.
25. Arshavsky VY, Lamb TD, Pugh EN, Jr (2002) G proteins and phototransductions. *Annu Rev Physiol* 64:153–187.
26. Baylor D (1996) How photons start vision. *Proc Natl Acad Sci USA* 93:560–565.
27. Detwiler PB, Ramanathan S, Sengupta A, Shraiman BI (2000) Engineering aspects of enzymatic signal transduction: Photoreceptors in the retina. *Biophys J* 79:2801–2817.
28. Trebak M, Lemonnier L, Smyth JT, Vazquez G, Putney JW, Jr (2007). Phospholipase C-coupled receptors and activation of TRPC channels. *Handb Exp Pharmacol* 179:593–614.
29. Zhang Y, *et al.* (2003) Coding of sweet, bitter and umami tastes: Different receptor cells sharing similar signaling pathways. *Cell* 112:293–301.